Design and Implementation of a Novel DC-DC Converter with Step-Up Ratio and Soft-Switching Technology

Kuei-Hsiang Chao * and Thi-Thanh-Truc Bau

Posted Date: 22 May 2025

doi: 10.20944/preprints202505.1715.v1

Keywords: high step-up converter; soft switching converter; zero voltage switching; coupled inductor; switching loss

 doi:10.20944/preprints202505.1715.v1

Article

Design and Implementation of a Novel DC-DC Converter with Step-Up Ratio and Soft-Switching Technology

Kuei-Hsiang Chao [1,*] and Thi-Thanh-Truc Bau [2]

[1] Department of Electrical Engineering, National Chin-Yi University of Technology, Taichung 41170, Taiwan
[2] Graduate Institute, Prospective Technology of Electrical Engineering and Computer Science, National Chin-Yi University of Technology, Taichung 41170, Taiwan
* Correspondence: chaokh@ncut.edu.tw; Tel.: +886-4-2392-4505 (ext.7272); Fax: +886-4-2392-2156

Abstract: This paper focuses on the development of a high-conversion-efficiency DC/DC boost converter, which features high step-up conversion and employs soft switching technology to reduce conversion losses. In the proposed design, the conventional energy storage inductor used in traditional boost converters is replaced with a coupled inductor, and an additional boost circuit is introduced. This configuration allows the converter to achieve a higher voltage conversion ratio under the same duty cycle, thereby enhancing the voltage gain of the converter. Additionally, a resonance branch is incorporated into the converter, and by applying a simple switching signal control, zero voltage switching (ZVS) of the main switch is realized. This reduces the switching loss inherent in hard switching high step-up converters, thereby improving the overall conversion efficiency. To validate the performance of the proposed converter, the circuit principle of the proposed high step-up soft switching converter is first analyzed, followed by the design of the circuit components. Subsequently, the feasibility of the proposed converter is verified using PSIM simulation software. Finally, the proposed high step-up soft switching boost converter is tested using the TMS320F2809 digital signal processor, and it is verified that the main switch successfully achieves ZVS. The converter operates under a full load of 340W, achieving a conversion efficiency of 92.7%, demonstrating the excellent conversion performance of the developed converter.

Keywords: high step-up converter; soft switching converter; zero voltage switching; coupled inductor; switching loss

1. Introduction

In recent years, renewable energy has gained increasing attention, with photovoltaic power generation system becoming one of the most widely applied forms of renewable energy. These systems are characterized by sustainable energy supply and minimal environmental impact. With advancements in technology, the installation and operational costs of photovoltaic power generation systems have continuously decreased, and their long-term maintenance costs are also relatively low, making them an ideal energy supply option. Additionally, with the rapid development of power electronics technology, converters play a crucial role in photovoltaic power generation systems, as they can significantly improve the energy conversion efficiency of the system. The primary function of a converter is to convert the direct current (DC) generated by the photovoltaic module array into alternating current (AC) or other DC values, for use in the power grid or energy storage. Due to the relatively low voltage output of photovoltaic modules and the need for subsequent applications in high-voltage systems, boost converters [1–3] are commonly used in photovoltaic power generation systems. However, boost converters also have certain drawbacks. When the switch is operated within a reasonable duty cycle, in order to prevent overheating and damage to the switch during prolonged operation, the voltage gain of the converter is limited, thus failing to meet the requirement for high output voltage. Moreover, if the switching frequency is too high

 doi:10.20944/preprints202505.1715.v1

when operating the switch, it results in significant switching losses. Although soft switching technologies [4–7] can reduce switching losses, they increase the size and cost of the converter and still cannot achieve the required higher output voltage. These issues affect the overall performance and cost-effectiveness of the photovoltaic power generation system.

In recent years, many researchers have begun to explore high step-up converters [8–11] to address the drawbacks of traditional boost converters. High step-up converters can convert the relatively low output voltage from a photovoltaic module array to a higher voltage, thereby reducing energy losses and improving system efficiency. However, this technology also faces several challenges. The design of high step-up converters is more complex and requires advanced electronic components and control techniques, which leads to increased manufacturing costs and greater risks to system reliability. Additionally, high step-up converters operate in high-voltage environments, posing potential voltage breakdown and insulation issues. Therefore, special insulation designs and protection measures are necessary. The boost converter presented in reference [8] demonstrates excellent step-up performance. However, due to the use of a three-winding coupled inductor, which increases the voltage gain through the turns ratio, the converter's physical size becomes significantly larger. In addition, the main switch in this converter does not achieve soft switching, resulting in higher switching losses during transitions between the on and off states. Furthermore, as the output voltage increases, the main switch must withstand higher voltage and current levels, significantly reducing the switch's lifespan. Reference [9] proposes a multi-stage series connection to increase the voltage gain; but the conversion efficiency decreases as the number of stages increases. Reference [10] presents an inductively coupled soft switching bidirectional converter, which offers a high step-up ratio and reduces input voltage ripple. However, it requires five switch components and six capacitors, which increases the size and cost of the physical hardware. Reference [11] introduces an interleaved high voltage ratio boost converter with coupled inductor. However, during the interleaved operation, the inactive converter still transmits some power, which reduces the overall efficiency and causes distortion in the average current. Reference [12] proposed an inductively coupled soft-switching bidirectional converter that also achieves a high step-up ratio. However, its main switch components must withstand higher voltage switching stresses, requiring switches with higher voltage ratings.

To address the drawbacks of the aforementioned converters, this paper proposes a high step-up soft switching converter. This converter uses a coupled inductor to replace the conventional energy storage inductor and incorporates a boost circuit, enabling a higher voltage conversion ratio under the same duty cycle, thereby improving the voltage gain of the converter. In addition, this paper incorporates a resonance branch into the converter and uses a simple switch signal control to achieve ZVS of the main switch, reducing switching losses in hard switching high step-up converters and improving conversion efficiency. First, the circuit architecture of the proposed converter was established using PSIM simulation software [13], and its feasibility was verified through simulation analysis. Finally, the implementation was carried out using the TMS320F2809 digital signal processor [14] from Texas Instruments, which demonstrated the superior conversion performance of the high step-up soft-switching converter.

2. The Proposed High Step-Up Converter

2.1. Operating Principle of the High Step-Up Hard Switching Converter

Figure 1 depicts the circuit architecture of the proposed high step-up hard-switching converter. This design replaces the traditional energy storage inductor with a coupled inductor and incorporates an additional boost circuit formed by D_1 and C_1. By leveraging the turns ratio of the coupled inductor and the boost circuit, the voltage conversion ratio is significantly enhanced. Furthermore, the converter features a simple circuit structure and ease of control, making it advantageous for practical applications. The operation of the converter can be divided into two modes based on the state of the switch (on and off). When the switch is on, the duty cycle D of the converter during one period T is defined by Equation (1).

 doi:10.20944/preprints202505.1715.v1

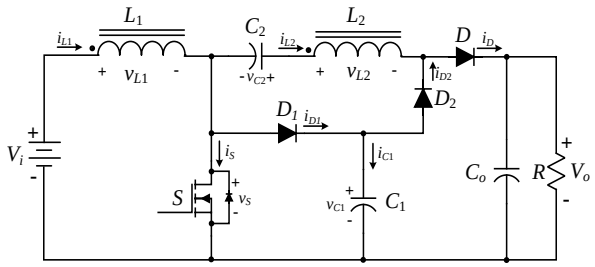

Figure 1. Circuit diagram of the high step-up hard switching converter.

$$D \triangleq \frac{t_{\text{on}}}{T} = \frac{t_{\text{on}}}{t_{\text{on}} + t_{\text{off}}} \tag{1}$$

Where t_{on} is the time during which the switch is conducting within one period, and t_{off} is the time during which the switch is off.

(1) Switch on ($0 \le t_{\text{on}} \le DT$)

When the switch S is conducting, the diode D_2 is also conducting, while the diode D and D_1 are in the off state. The equivalent circuit is shown in Figure 2, and the turns ratio N of the coupled inductor is defined by Equation (2). At this point, the inductor voltages v_{L1} and v_{L2} are expressed by Equations (3) and (4), respectively, while the voltage v_{C2} across the energy storage capacitor C_2, is given by Equation (5).

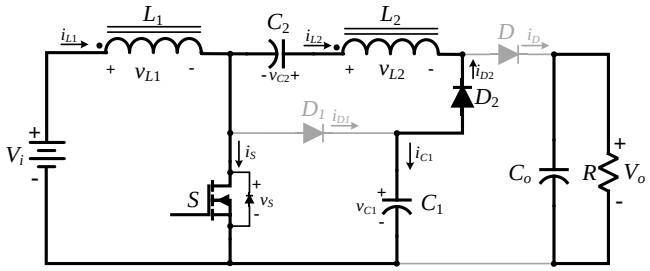

Figure 2. Equivalent circuit when the main switch S is conducting in the high step-up hard switching converter.

$$N \triangleq \frac{N_2}{N_1} \tag{2}$$

$$v_{L1} = V_i \tag{3}$$

$$v_{L2} = \frac{N_2}{N_1} V_i = NV_i \tag{4}$$

$$v_{C2} = v_{L2} + v_{C1} = V_i \left(N + \frac{1}{1-D} \right) \tag{5}$$

(2) Switch off ($DT \le t_{\text{off}} \le T$)

When the switch S is off, diode D_2 is in the off state, while diodes D and D_1 are conducting. The equivalent circuit is shown in Figure 3, and the inductor voltages v_{L1} and v_{L2} are given by Equations (6) and (7), respectively.

 doi:10.20944/preprints202505.1715.v1

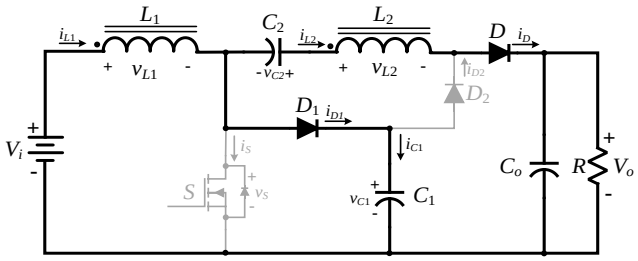

Figure 3. Equivalent circuit of the high step-up hard switching converter when the main switch *S* is off.

$$v_{L1} = V_i - v_{C1} = -V_i \frac{D}{1-D} \tag{6}$$

$$v_{L2} = V_i + v_{C2} - v_{L1} - V_o = NV_i + 2\frac{V_i}{1-D} - V_o \tag{7}$$

Based on the volt-second balance theorem for the inductor L_2 , the Equations (4) and (7) lead to Equation (8). After simplification, the voltage conversion ratio between the output voltage V_o and the input voltage V_i can be expressed by Equation (9).

$$NV_i DT + (NV_i + 2\frac{V_i}{1-D} - V_o)(1-D)T = 0 \tag{8}$$

$$G = \frac{V_o}{V_i} = \frac{2+N}{1-D} \tag{9}$$

From Equation (9), the relationship between the voltage gain of the converter and the duty cycle is shown in Table 1. From Table 1 and Figure 4, it can be observed that, for the same duty cycle, the voltage conversion ratio of the converter can be increased by adjusting the turns ratio of the coupled inductor.

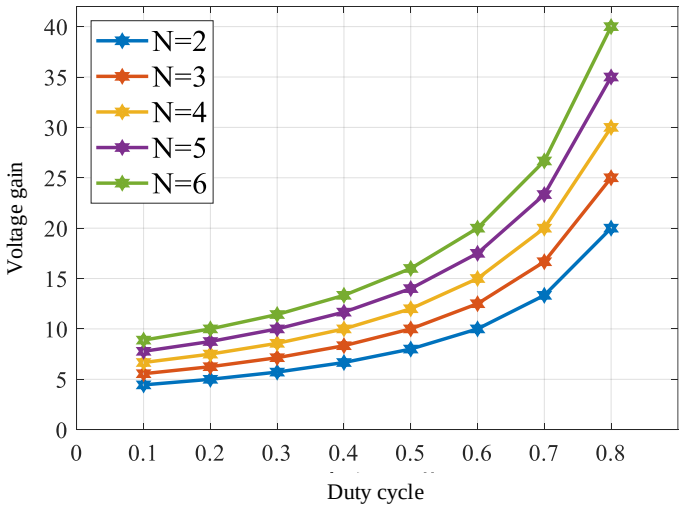

Figure 4. Voltage gain vs. duty cycle curve for high step-up hard switching converter.

 doi:10.20944/preprints202505.1715.v1

Table 1. Relationship between voltage gain and duty cycle for the high step-up hard switching converter.

Duty Cycle \ Turns Ratio	*N*=2	*N*=3	*N*=4	*N*=5	*N*=6
D=0.1	*G*=4.4	*G*=5.6	*G*=6.7	*G*=7.8	*G*=8.9
D=0.2	*G*=5	*G*=6.3	*G*=7.5	*G*=8.8	*G*=10
D=0.3	*G*=5.7	*G*=7.1	*G*=8.6	*G*=10	*G*=11.4
D=0.4	*G*=6.7	*G*=8.3	*G*=10	*G*=11.7	*G*=13.3
D=0.5	*G*=8	*G*=10	*G*=12	*G*=14	*G*=16
D=0.6	G=10	*G*=12.5	*G*=15	*G*=17.5	*G*=20
D=0.7	*G*=13.3	*G*=16.7	*G*=20	*G*=23.3	*G*=26.7
D=0.8	*G*=20	*G*=25	*G*=30	*G*=35	*G*=40

2.2. Operating Principle of the High Step-Up Hard Switching Converter

The high step-up hard switching converter described above can increase the converter's voltage conversion ratio by utilizing a coupled inductor and an additional boost circuit. However, if the voltage or current cannot be reduced to zero before switching occurs, switching losses will arise, which in turn lowers the overall efficiency of the converter. To improve the conversion efficiency, this paper proposes a high step-up soft switching converter with an inductive coupling. The circuit architecture of this converter is shown in Figure 5, while Figure 6 illustrates the switching control signals for the converter [15]. The converter achieves a high voltage conversion ratio through inductive coupling and an additional boost circuit. It also incorporates a resonant branch composed of L_r, C_1 and S_r, where C_1 is the capacitor originally used in the hard switching converter circuit. By controlling the switching signals, the converter enables ZVS for the main switch, thus improving efficiency and reducing switching losses. This paper will analyze the operating modes of the proposed soft switching converter, which is divided into nine distinct modes. Figure 7 shows the switching waveforms for each component. Before explaining the operating modes, the following assumptions are made:

1) The converter operates in continuous conduction mode (CCM), and the circuit has reached a steady state.

2) All components are ideal, meaning that during conduction they are treated as short circuits, and during cutoff, as open circuits. Consequently, there is no conduction voltage drop across the power switching components.

3) The input and output voltages are maintained at constant values.

4) The currents of the energy storage inductors L_1 and L_2 are considered constant (i.e. $i_{L1} = I_{L1}$, $i_{L2} = I_{L2}$).

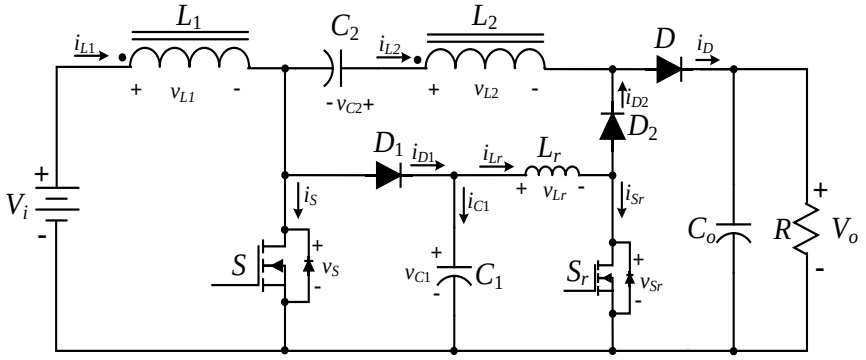

Figure 5. Circuit architecture of the proposed high step-up soft switching converter.

 doi:10.20944/preprints202505.1715.v1

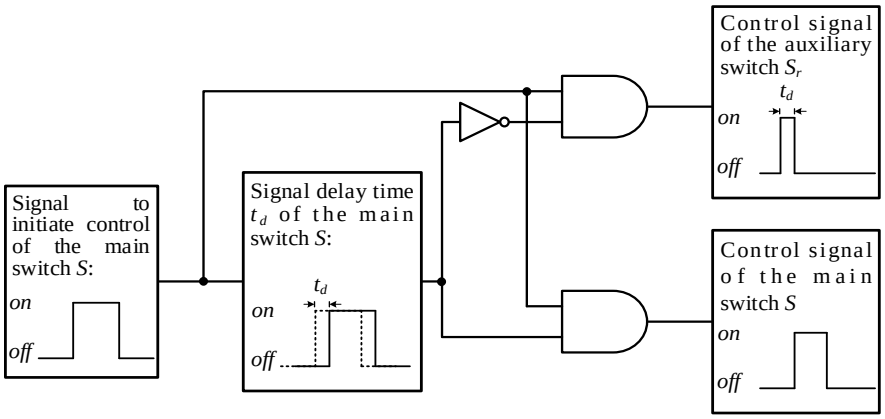

Figure 6. Switching signal diagram of the high step-up soft switching converter [15].

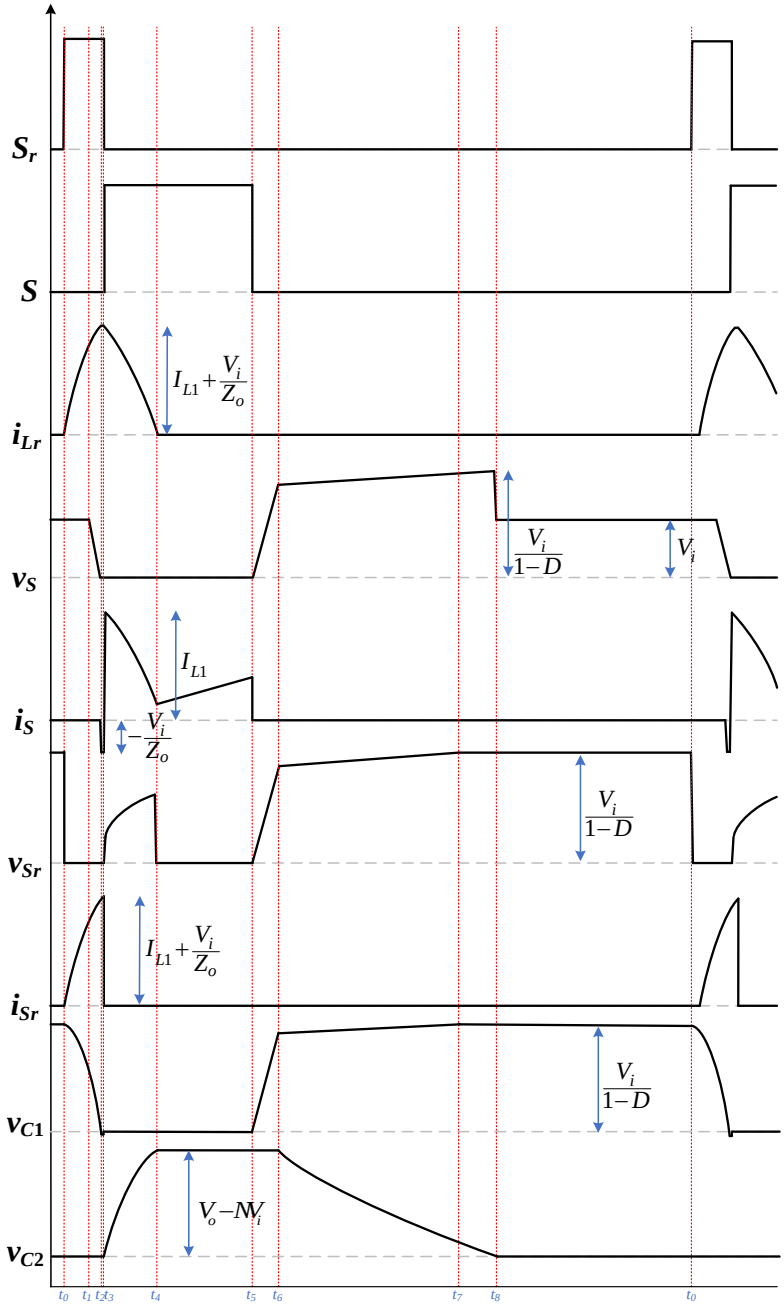

Figure 7. Switching waveforms of each component in the proposed converter under different operating modes.

 doi:10.20944/preprints202505.1715.v1

(1) Mode 1 ($t_0 \sim t_1$)

When operating in Mode 1, the equivalent circuit is shown in Figure 8. In this mode, the main switch S is in the off state, while the auxiliary switch S_r is turned on first. As a result, the resonant capacitor C_1 begins to discharge, and the voltage across the resonant inductor L_r is v_{C1}. The current through the resonant inductor i_{Lr} rises from zero. Therefore, the resonant inductor L_r and resonant capacitor C_1 form a resonant tank, and the circuit equations can be expressed by Equation (10). After solving, the i_{Lr} and v_{C1} are given by Equation (11), while the resonant impedance Z_o and resonant angular frequency ω_o are given by Equation (12). When the voltage v_{C1} across the resonant capacitor drops to V_i, diode D_1 switches from the off state to the on state. The circuit then transitions to Mode 2. The time for this transition is given by Equation (13).

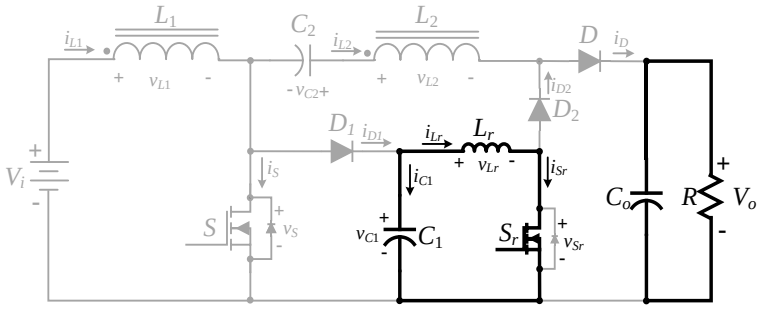

Figure 8. Circuit conduction state in Mode 1.

$$\begin{cases} i_{Lr}(t_o) = 0 \\ v_{C1}(t_o) = \dfrac{V_i}{1-D}, \quad t_0 \le t \le t_1 \\ i_{C1}(t) = -i_{Lr}(t) \\ v_{C1}(t) = v_{Lr}(t) \end{cases} \tag{10}$$

$$\begin{cases} i_{Lr}(t) = \dfrac{V_i}{(1-D)Z_o}\sin\omega_o(t-t_o) \\ v_{C1}(t) = \dfrac{V_i}{1-D}\cos\omega_o(t-t_o) \end{cases}, \quad t_0 \le t \le t_1 \tag{11}$$

Where the resonance impedance $Z_o \triangleq \sqrt{\dfrac{L_r}{C_1}}$ and resonance frequency

$$\omega_o \triangleq \frac{1}{\sqrt{L_r C_1}} \tag{12}$$

$$T_1 = t_1 - t_o = \sqrt{L_r C_1}\cos^{-1}(1-D) \tag{13}$$

(2) Mode 2 ($t_1 \sim t_2$)

When entering working Mode 2, the equivalent circuit is shown in Figure 9. At this point, the voltage across the resonant capacitor v_{C1} has decreased to V_i. At this point, the auxiliary switch S_r remains on, and both the resonant inductor L_r and the resonant capacitor C_1 continue to form a resonant circuit. The resonant inductor current i_{Lr} will continue to increase, and the resonant capacitor C_1 will keep discharging. The circuit equations for this mode can be expressed as Equation (14). From Equation (14), $i_{Lr}(t)$ and $v_{C1}(t)$ can be derived as shown in Equation (15). When the voltage across the resonant v_{C1} capacitor drops to zero, at which point $\omega_o(t-t_1) = \dfrac{\pi}{2}$, the resonant inductor current i_{Lr} can be calculated from Equation (15) as shown in Equation (16). The operating time for this

 doi:10.20944/preprints202505.1715.v1

mode can be derived as shown in Equation (17). At this point, the anti-parallel diode of the main switch *S* will begin to conduct, and the system will enter working Mode 3.

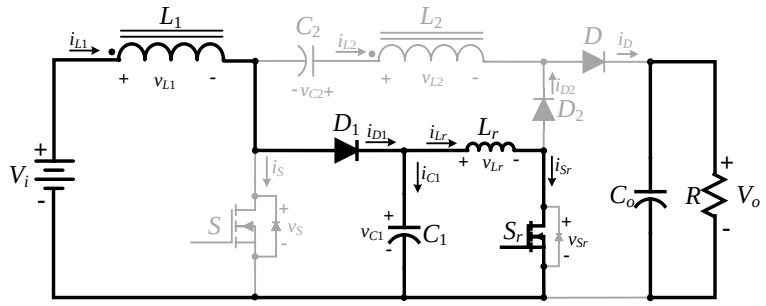

Figure 9. Circuit conduction state in Mode 2.

$$\begin{cases} i_{Lr}(t) + C_1 \dfrac{dv_{C1}(t)}{dt} = I_{L1} \\ L_r \dfrac{di_{Lr}(t)}{dt} = v_{C1}(t) \\ v_{C1}(t_1) = V_i \end{cases}, \quad t_1 \le t \le t_2 \tag{14}$$

$$\begin{cases} i_{Lr}(t) = I_{L1} + \dfrac{V_i}{Z_o}\sin\omega_o(t-t_1) \\ v_{C1}(t) = V_i\cos\omega_o(t-t_1) \end{cases}, \quad t_1 \le t \le t_2 \tag{15}$$

$$i_{Lr}(t_2) = i_{Sr}(t_2) = I_{L1} + \frac{V_i}{Z_o} \tag{16}$$

$$T_2 = t_2 - t_1 = \frac{\pi}{2}\sqrt{L_r C_1} \tag{17}$$

(3) Mode 3 ($t_2 \sim t_3$)

When the system enters working Mode 3, the equivalent circuit is shown in Figure 10. At this point, the voltage across the resonant capacitor v_{C1} has dropped to a very small negative voltage, which causes the anti-parallel diode of the main switch *S* to forward conduct. As a result, the voltage across the main switch *S* is zero. The control of the main switch *S* is then switched from the off state to the on state, achieving ZVS for the main switch *S*. At the same time, the auxiliary switch S_r is switched off. The circuit equations for this mode can be expressed as Equation (18). To ensure ZVS for the main switch, the delay time t_d must satisfy the condition in Equation (19), and typically t_d is 5% to 10% of the switching period *T*. Moreover, to ensure that the main switch *S* can still achieve ZVS under heavy load conditions, and considering the turn-off speed of the auxiliary switch S_r, an additional time delay t_a must be considered. Thus, the operating time t_{DSr} of the auxiliary switch can be expressed as shown in Equation (20).

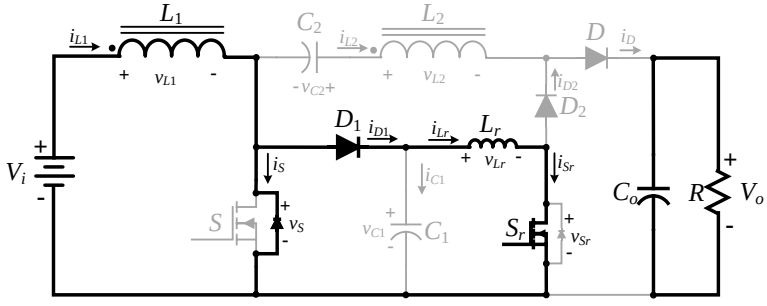

Figure 10. Circuit conduction state in Mode 3.

 doi:10.20944/preprints202505.1715.v1

$$\begin{cases} i_S(t_2) = I_{L1} - i_{Lr}(t_2) = -\dfrac{V_i}{Z_o} \\ i_{Lr}(t_2) = I_{L1} + \dfrac{V_i}{Z_o} \end{cases}, \quad t_2 \le t \le t_3 \tag{18}$$

$$t_d \ge T_1 + T_2 = \sqrt{L_r C_1}\left(\frac{\pi}{2} + \cos^{-1}(1-D)\right) \tag{19}$$

$$t_{DSr} \ge t_d + t_\alpha = \sqrt{L_r C_1}\left(\frac{\pi}{2} + \cos^{-1}(1-D)\right) + t_\alpha \tag{20}$$

(4) Mode 4 ($t_3 \sim t_4$)

In Mode 4, the main switch S is conducting, while the auxiliary switch S_r switches off. Diodes D_1 and D_2 are forward-biased, and the equivalent circuit is shown in Figure 11. In this mode, to allow the energy storage capacitor C_2 and the resonant inductor L_r to form a resonant tank, the capacitance of C_2 is chosen to be close to that of C_1. Additionally, the resonant inductor L_r and the common-mode inductance L_2 both discharge into the energy storage capacitor C_2. At this point, the current through the resonant inductor L_r is $I_{L1} + \dfrac{V_i}{Z_o}$. The circuit equation for this mode can be expressed as Equation (21). Solving for $i_{Lr}(t)$ and $v_{C2}(t)$ gives Equation (22). In this working mode, the current through the resonant inductor i_{Lr} decreases from $I_{L1} + \dfrac{V_i}{Z_o}$ to zero, and diodes D_1 and D_2 switch off. The circuit then transitions into Mode 5.

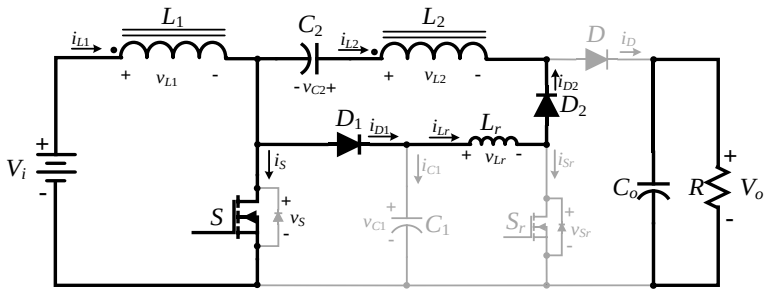

Figure 11. Circuit conduction state in Mode 4.

$$\begin{cases} L_r \dfrac{di_{Lr}(t)}{dt} = v_{L2}(t) - v_{C2}(t) \\ C_2 \dfrac{dv_{C2}(t)}{dt} = i_{Lr}(t) \\ v_{L2}(t) = N v_{L1}(t) = N V_i \\ v_{C1}(t_3) = 0 \\ i_{Lr}(t_4) = 0 \end{cases}, \quad t_3 \le t \le t_4 \tag{21}$$

$$\begin{cases} i_{Lr}(t) = \left(I_{L1} + \dfrac{V_i}{Z_o}\right)\cos\omega_o(t-t_3) + \dfrac{NV_i}{Z_o}\sin\omega_o(t-t_3) \\ v_{C2}(t) = NV_i\left[1+\cos\omega_o(t-t_3)\right] + \left(I_{L1} + \dfrac{V_i}{Z_o}\right)\sin\omega_o(t-t_3) \end{cases} \tag{22}$$

(5) Mode 5 ($t_4 \sim t_5$)

In Mode 5, the equivalent circuit is shown in Figure 12. At this point, the main switch S remains conducting. The circuit equation for this mode can be expressed as Equation (23). This mode continues until the main switch S transitions from conducting to off.

 doi:10.20944/preprints202505.1715.v1

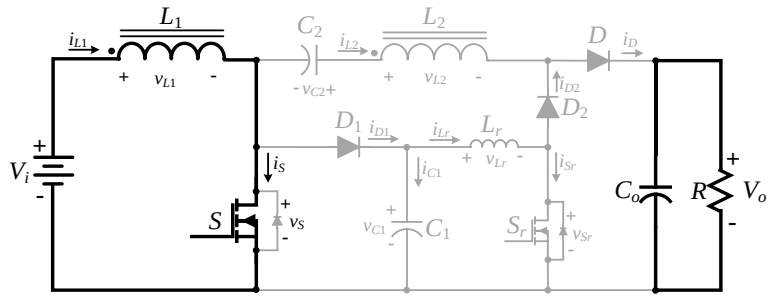

Figure 12. Circuit conduction state in Mode 5.

$$\begin{cases} i_S(t) = I_{L1} \\ v_{C1}(t) = 0 \end{cases}, \quad t_4 \le t \le t_5 \tag{23}$$

(6) Mode 6 ($t_5 \sim t_6$)

In Mode 6, the main switch S is turned off and the equivalent circuit is shown in Figure 13. As a result, the current I_{L1} charges the resonant capacitor C_1, causing the voltage across the resonant capacitor v_{C1} to gradually increase. The circuit equation for this mode is given by Equation (24). By solving Equation (24), $v_{C1}(t)$ can be obtained as Equation (25). When the resonant capacitor voltage v_{C1} reaches V_i, this mode ends and transitions into Mode 7. Therefore, the operating time for this mode can be determined from Equation (26).

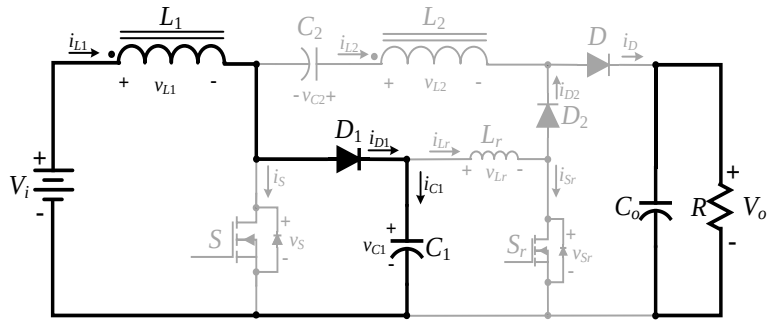

Figure 13. Circuit conduction state in Mode 6.

$$C_1 \frac{dv_{C1}(t)}{dt} = I_{L1}, \quad t_5 \le t \le t_6 \tag{24}$$

$$v_{C1}(t) = \frac{I_{L1}}{C_1}(t - t_5) \tag{25}$$

$$T_6 = t_6 - t_5 = \frac{V_i C_1}{I_{L1}} \tag{26}$$

(7) Mode 7 ($t_6 \sim t_7$)

In Mode 7, the voltage across the resonant capacitor v_{C1} is V_i, and the main switch S remains in the off state, while the auxiliary switch S_r is also off. As a result, the coupled inductor L_2 and the energy storage capacitor C_2 transfer energy to the load via diode D. The circuit equation for this mode is given by Equation (27), and the equivalent circuit is shown in Figure 14. By solving Equation (27), the voltage v_{C1} across the resonant capacitor C_1 can be obtained as Equation (28). At this point, the current flowing through the coupled inductor I_{L1} and the current I_{L2} gradually decrease, and when the currents I_{L1} and I_{L2} become equal, the circuit transitions into Mode 8.

 doi:10.20944/preprints202505.1715.v1

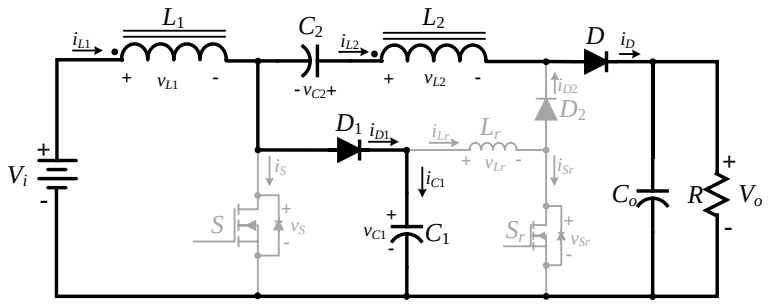

Figure 14. Circuit conduction state in Mode 7.

$$\begin{cases} C_1 \dfrac{\mathrm{d}v_{C1}}{\mathrm{d}t} = I_{L1} - I_{L2} \\ v_{C1}(t_6) = V_i \end{cases}, \quad t_6 \le t \le t_7 \tag{27}$$

$$v_{C1}(t) = \frac{I_{L1} - I_{L2}}{C_1}(t - t_6), \quad t_6 \le t \le t_7 \tag{28}$$

(8) Mode 8 ($t_7 \sim t_8$)

In Mode 8, the voltage across the resonant capacitor v_{C1} is $V_i / (1-D)$, and diode D_1 transitions from the conducting to the off state. The resonant capacitor C_1 stops charging, and both the main switch S and the auxiliary switch S_r remain off. Consequently, the coupled inductor and the energy storage capacitor C_2 continue to transfer energy to the load. The equivalent circuit for this mode is shown in Figure 15, and the circuit equation is given by Equation (29). When the voltage across the energy storage capacitor C_2 drops to zero, this mode ends, and the circuit transitions into Mode 9.

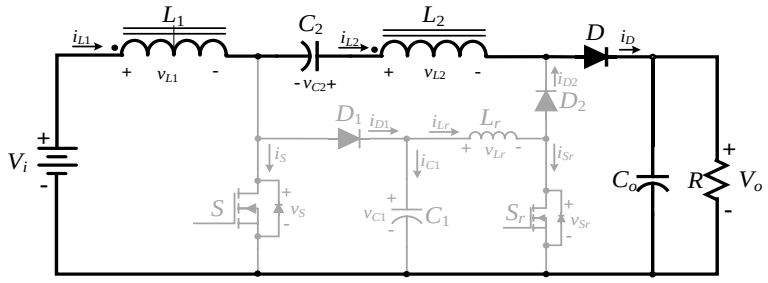

Figure 15. Circuit conduction in Mode 8.

$$\begin{cases} I_{L1} = I_{L2} \\ v_{C1}(t_7) = \dfrac{V_i}{1-D} \end{cases}, \quad t_6 \le t \le t_7 \tag{29}$$

(9) Mode 9 ($t_8 \sim t_9$)

In Mode 9, the voltage across the energy storage capacitor v_{C2} is zero, and diode D transitions from conducting to the off state. Both the main switch S and the auxiliary switch S_r remain off. The equivalent circuit for this mode is shown in Figure 16, marking the completion of the entire switching cycle analysis. The cycle will repeat once the auxiliary switch S_r turns on again, returning to Mode 1 of the next cycle.

 doi:10.20944/preprints202505.1715.v1

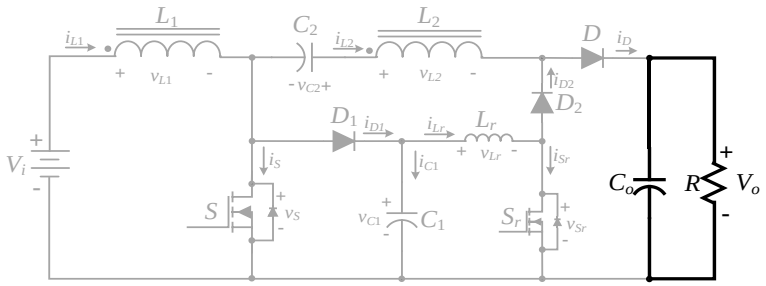

Figure 16. Circuit conduction state in Mode 9.

To demonstrate the performance of the proposed high step-up soft switching converter, a comparison is made with various high step-up soft switching converters. The comparison is based on voltage gain, switch voltage ratings, number of switching components, number of diode components, number of inductive components, and number of capacitive components. The results are summarized in Table 2. As shown in the table, the proposed converter achieves a high voltage gain with fewer components and utilizes simple signal control for soft switching, highlighting its key advantages.

Table 2. Component specifications of the high voltage ratio soft switching converter adopted.

Converter Topology	Converter in [4]	Converter in [5]	Converter in [6]	Converter in [12]	Proposed Converter
Voltage Gain	$\frac{2N+2-ND}{1-D}$	$\frac{2+N}{1-D}$	$\frac{2+N}{1-D}$	$\frac{2N+2-ND}{1-D}$	$\frac{2+N}{1-D}$
Voltage Stress on MOSFETs	$\frac{V_O}{2N+2-ND}$	$\frac{V_O}{2+N}$	$\frac{V_O}{2+N}$	$\frac{V_O-NV_i}{1+2N}$	$\frac{V_i}{1-D}$
MOSFETs	2	4	2	2	2
Diodes	3	0	2	3	3
Inductors	1	1	2	2	2
Capacitors	4	4	4	3	3

3. Component Design of the Proposed High Step-Up Converter

The output power of the high step-up hard switching converter proposed in this paper is 340W. The relevant circuit parameters and specifications are provided in Table 3.

Table 3. Parameter specifications of the high step-up hard-switching converter.

Input Voltage V_i	72 V ± 10%
Output Voltage V_o	430 V
Output Power P_o	340 W
Switching Frequency f	25 kHz
Turns Ratio of Coupling Inductor N	2

In the case where all components are operating under ideal conditions, the input power should be equal to the output power, i.e.

$$V_i I_{L1} = \frac{V_o^2}{R} \tag{30}$$

$$I_{L1} = \frac{V_o^2}{V_i^2}\frac{V_i}{R} \tag{31}$$

Substituting Equation (9) into Equation (31) yields, as expressed in Equation (32).

 doi:10.20944/preprints202505.1715.v1

$$I_{L1} = \left(\frac{2+N}{1-D}\right)^2 \frac{V_i}{R} \tag{32}$$

where $\frac{2+N}{1-D}$ represents the voltage gain of the converter.

When the main switch *S* is turned on, v_{L1} can be expressed as:

$$v_{L1} = V_i = L_1 \frac{\mathrm{d}i_{L1}}{\mathrm{d}t} \tag{33}$$

From Equation (33), it can be observed that when the main switch is turned on, the inductor current i_{L1} increases linearly, with the conduction time denoted as $t_{on} = DT$. The rate of change of the inductor current can be calculated as shown in Equation (34).

$$\Delta i_{L1(\text{close})} = \frac{V_i}{L_1} DT \tag{34}$$

Using Equations (32) and (34), the maximum and minimum values of the inductor current i_{L1} can be derived, as expressed in Equations (35) and (36) [16].

$$I_{L1(\max)} = I_{L1} + \frac{\Delta i_{L1}}{2} = \left(\frac{2+N}{1-D}\right)^2 \frac{V_i}{R} + \frac{V_i D}{2L_1 f} \tag{35}$$

$$I_{L1(\min)} = I_{L1} - \frac{\Delta i_{L1}}{2} = \left(\frac{2+N}{1-D}\right)^2 \frac{V_i}{R} - \frac{V_i D}{2L_1 f} \tag{36}$$

If $I_{L1(\min)} = 0$, the inductor can operate at the boundary between CCM and discontinuous conduction mode, which yields:

$$\left(\frac{2+N}{1-D}\right)^2 \frac{V_i}{R} = \frac{V_i D}{2L_{1(\min)} f} \tag{37}$$

From Equation (37), the value of $L_{1(\min)}$ can be calculated as:

$$L_{1(\min)} = \frac{DR}{2f}\left(\frac{1-D}{2+N}\right)^2 \tag{38}$$

Since the coupled inductor structure is similar to the coupled transformer structure, the maximum value of I_{L2} can be shown as [16]:

$$I_{L2(\max)} = -\frac{I_{L1(\max)}}{1+N} \tag{39}$$

3.1. Design of Coupled Inductors

The given scenario involves ensuring that a converter operates in CCM across all duty cycles, with a maximum output power of 340W, a fixed output voltage of 430V, and a rated load of 550Ω. From the relationship between the duty cycle *D* and the $\frac{D}{2}\left(\frac{1-D}{2+N}\right)^2$ function curve shown in Figure 17, it is observed that the function $\frac{D}{2}\left(\frac{1-D}{2+N}\right)^2$ reaches its maximum value when *D*=0.33. By substituting the load resistance *R*=550Ω, the turns ratio of the coupled inductors *N*=2, the switching frequency *f*=25kHz, and the duty cycle *D*=0.33 into Equation (38), the minimum primary inductance $L_{1(\min)}$ of the coupled inductor is calculated to be 102μH. To ensure that the coupling inductor L_1 operates in CCM under both light and heavy load conditions, the calculated inductance value is further multiplied by a safety factor of 1.25. Hence, the selected value of the coupling inductor L_1 is 127 μH.

 doi:10.20944/preprints202505.1715.v1

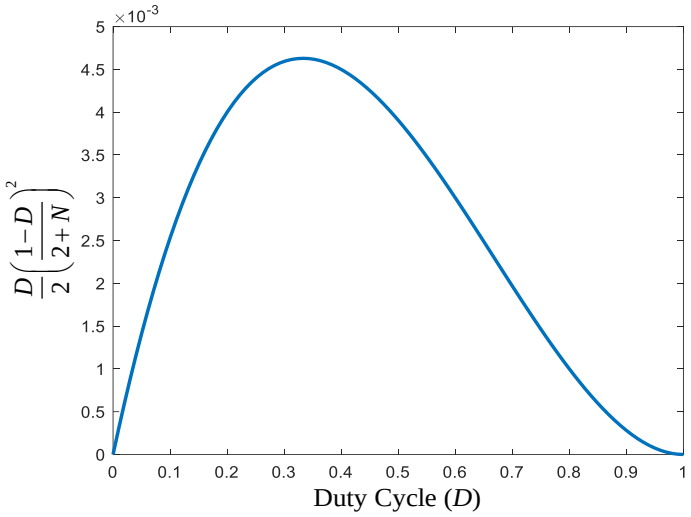

Figure 17. The relationship curve between the duty cycle D and the function $\frac{D}{2}\left(\frac{1-D}{2+N}\right)^2$.

3.2. Design of Capacitors C_1 and C_2

From Figure 1 of the high step-up hard switching converter, it can be observed that the capacitor C_1, coupled inductor L_1, main switch S, and diode D_1 form a traditional boost converter. When the duty cycle of the main switch S is 0.8, the voltage across capacitor C_1 is approximately 360V. From Equation (5), under the same operating conditions, the voltage across capacitor C_2 is around 500V. Therefore, the rated voltage of capacitor C_1 is selected as 400V, while the rated voltage of capacitor C_2 is 600V. Based on the analysis of operating Mode 3 in Equation (18) and Figure 7, it is evident that the capacitance value of C_1 influences the reverse current flowing through the main switch S. Considering ripple size and component availability, the chosen capacitance value for C_1 is 0.33μF/400V. Additionally, from the explanation of operating Mode 4 of this high step-up soft-switching converter, it is understood that C_2 should have a capacitance value similar to that of C_1, so C_2 is selected as 0.33μF/600V.

3.3. Design of Resonant Inductor L_r

Since the conduction time of the auxiliary switch in a typical soft switching converter is usually designed to be between 5% and 10% of the switching period, let $t_d = 10\%T = 4\mu s$ ($T = \frac{1}{f} = \frac{1}{25\text{kHz}} = 40\mu s$) and $t_\alpha = 2\%T = 0.8\mu s$ represent these values, respectively. From Equation (20), if the duty cycle D is set within the range of 0.1 to 0.8, the resonance inductance value can be calculated to vary between 8.08μH and 17.08μH. Based on this, the chosen resonance inductance for the converter is 18μH.

After the design of the aforementioned components, the specifications of the components used in the proposed high step-up soft-switching converter are listed in Table 4.

 doi:10.20944/preprints202505.1715.v1

Table 4. Parameter specifications of the high step-up hard-switching converter.

Component	Specifications
Coupled Inductor L_1	127μH
Resonant Inductor L_r	18μH
Main Switch S	MOSFET-TK49N65W(650V/49A)
Auxiliary Switch S_r	MOSFET-TK49N65W(650V/49A)
Fast Diodes (D, D_1, D_2)	IQBD30E60A1(600V/30A)
Filtering Capacitor C_o	340μF/900V
Resonant Capacitor C_1	0.33μF/400V
Energy Storage Capacitor C_2	0.33μF/600V

4. Simulation Results

The PSIM simulation software [13] was first used in this study to model the high step-up soft switching converter, in order to verify that the proposed converter achieves superior conversion performance under both light and full load conditions. Figure 18 shows the waveform of the duty cycle, input voltage, and output voltage when the converter operates at full load (P=340W). The output voltage of 430V is obtained when the input voltage is 72V and the duty cycle is 0.33, as shown in Figure 18. Therefore, the converter exhibits a high step-up ratio, and its voltage gain is consistent with the value listed in Table 1. Figure 19 and Figure 20 show the simulation waveforms of the electrical quantities for the main switch S and auxiliary switch S_r when the converter operates at full load (P=340W). Figure 21 and Figure 22 show the simulation waveforms of the electrical quantities for the main switch S and auxiliary switch S_r when the converter operates at light load (P=100W). From Figure 19 and Figure 21, it can be observed that at both full load (P=340W) and light load (P=100W), the voltage across the main switch S drops to zero before the switch enters the conduction mode. This demonstrates that the main switch S achieves ZVS, confirming that the proposed converter enables soft-switching for the main switch.

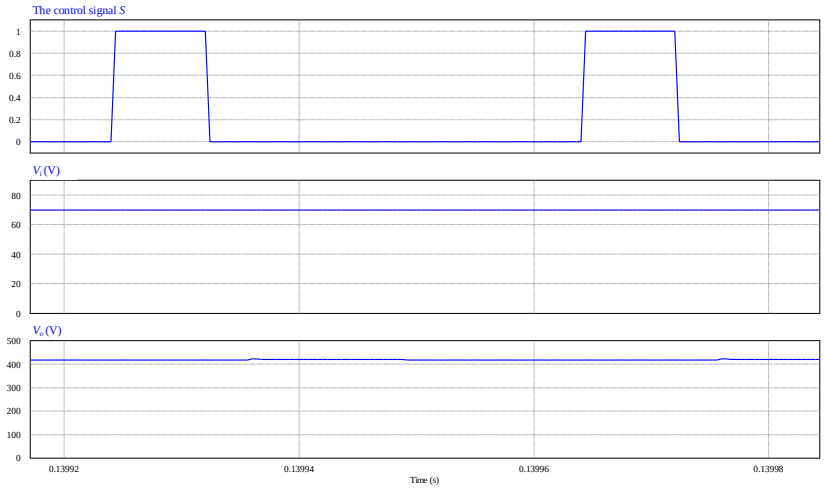

Figure 18. Main switch control signal duty cycle, input voltage, and output voltage waveforms of the converter operating at full load (P=340W).

 doi:10.20944/preprints202505.1715.v1

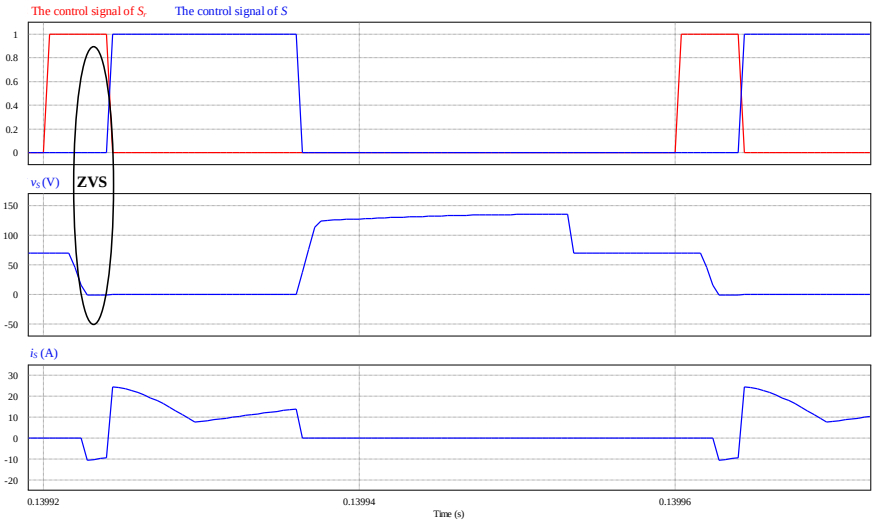

Figure 19. Simulation waveforms of the electrical quantities for the main switch S at full load (P=340W).

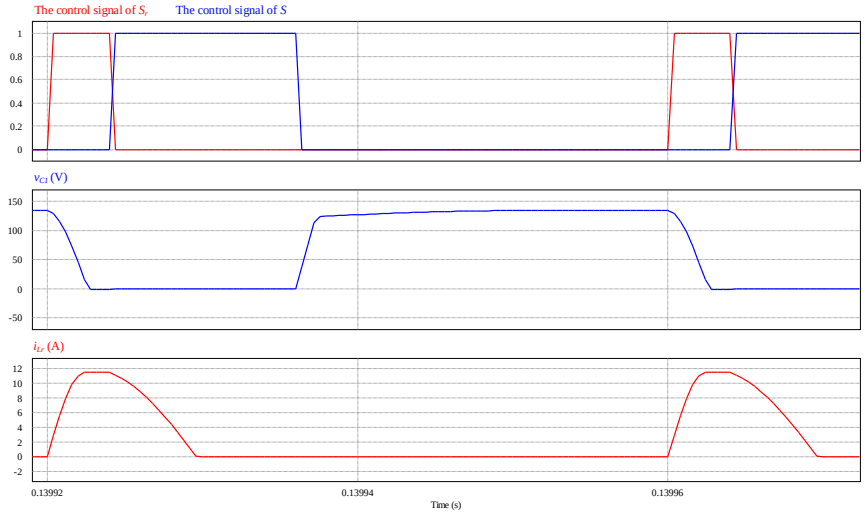

Figure 20. Simulation waveforms of the electrical quantities for the auxiliary switch S_r of the converter when operating at full load (P=340W).

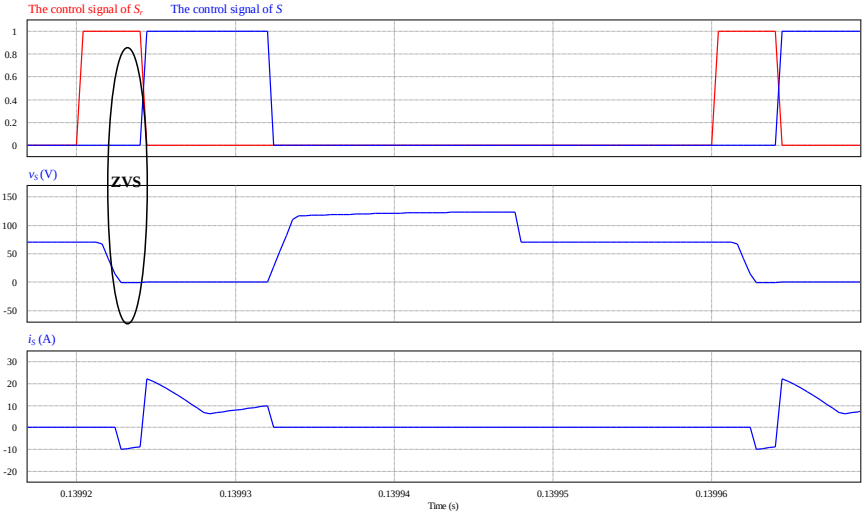

Figure 21. Simulation waveforms of the electrical quantities for the main switch S at light load (P=100W).

 doi:10.20944/preprints202505.1715.v1

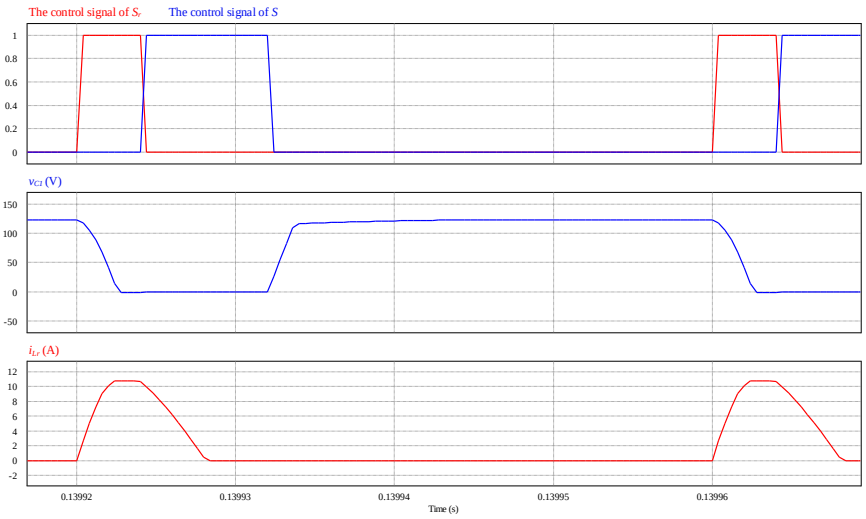

Figure 22. Simulation waveforms of the electrical quantities for the auxiliary switch S_r of the converter at light load (P=100W).

5. Experimental Results

After verifying the feasibility of the proposed converter using PSIM simulation software, the practical implementation of the high step-up soft switching converter was conducted using the TMS320F2809 [14] digital signal processor as the control core. The overall hardware circuit setup is shown in Figure 23, and the test platform is depicted in Figure 24. Figure 25 shows the waveforms of the trigger signal for the main switch S, input voltage, and output voltage of the high step-up soft-switching converter under full-load operation P=340W. From Figure 25, it can be observed that when the duty cycle of the main switch is 0.33 and the input voltage is 72V, the output voltage reaches 430V, achieving the expected voltage gain as shown in Table 1. Figures 26–29 show the waveforms of the trigger signals, voltages, and currents for the main switch S and auxiliary switch S_r at load conditions of P=100W and P=340W, respectively. The experimental results demonstrate that the proposed high step-up ratio soft switching converter achieves ZVS for the main switch S under both light load (P=100W) and full load (P=340W) conditions. This helps reduce the switching loss, thereby improving the overall conversion efficiency. Additionally, the measured waveforms of the main switch S and auxiliary switch S_r match the simulated waveforms. Figure 30 shows a comparison of the efficiency between the proposed high step-up soft-switching and hard-switching converters, with loads ranging from P=100W to P=340W. The figure demonstrates that the conversion efficiency improves by 3-4% across different load levels.

 doi:10.20944/preprints202505.1715.v1

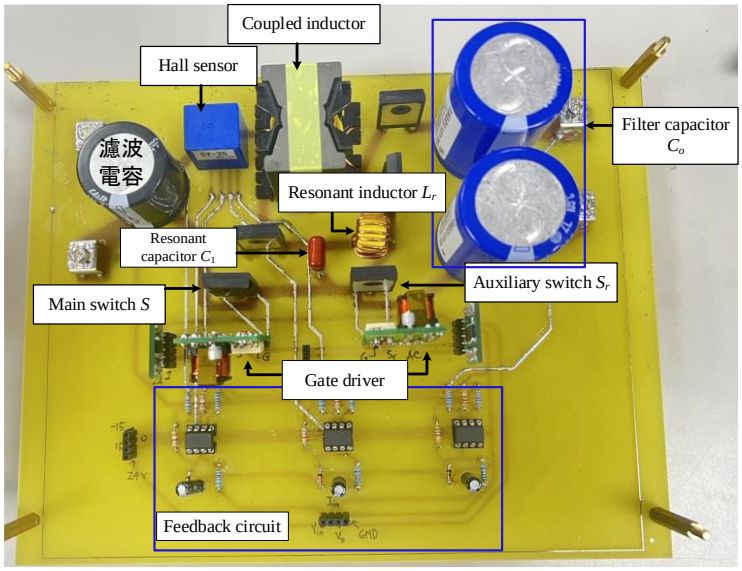

Figure 23. Physical appearance of the high step-up soft switching converter circuit.

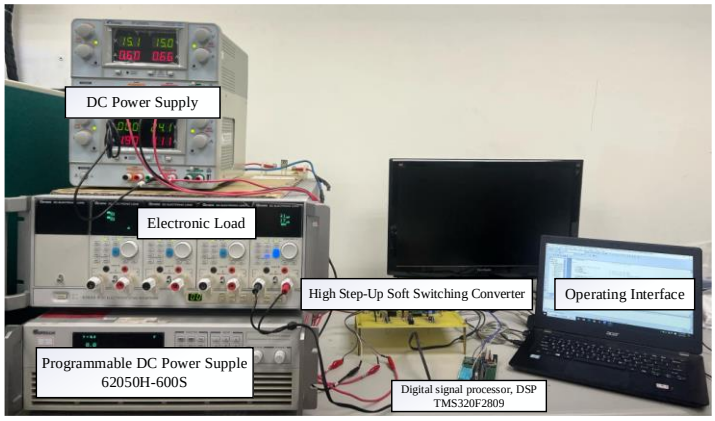

Figure 24. Test platform for the high step-up soft switching converter.

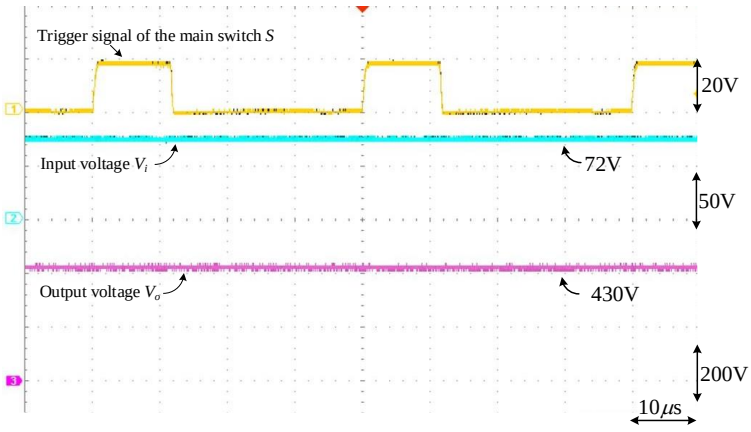

Figure 25. Waveform of the trigger signal, input voltage, and output voltage of the main switch S when the converter operates under full load (P=340W).

 doi:10.20944/preprints202505.1715.v1

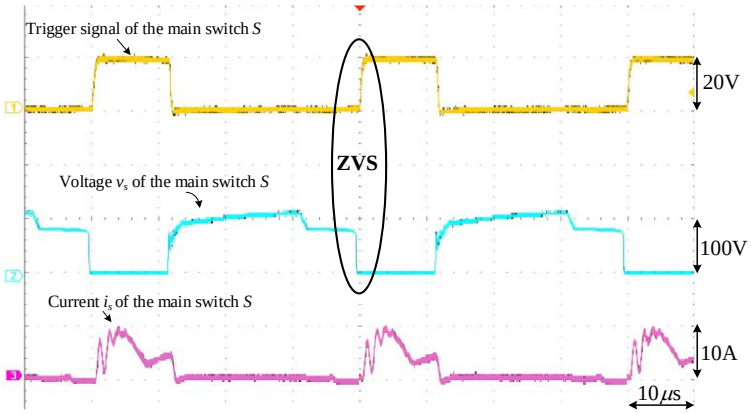

Figure 26. Waveform of the trigger signal, voltage, and current of the main switch *S* under light load (*P*=100W).

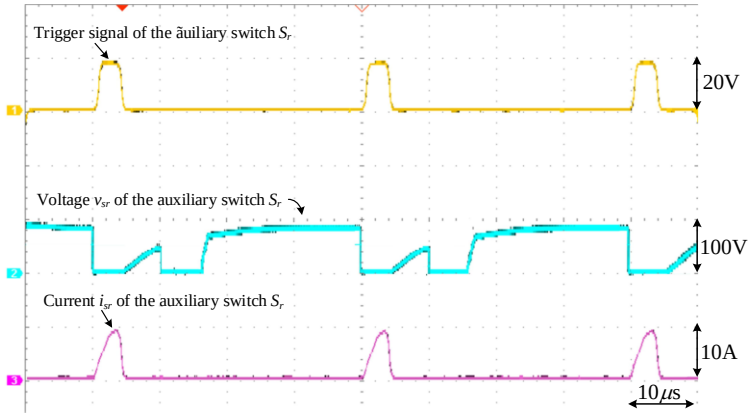

Figure 27. Waveform of the trigger signal, voltage, and current of the auxiliary switch S_r under full load (P=100W).

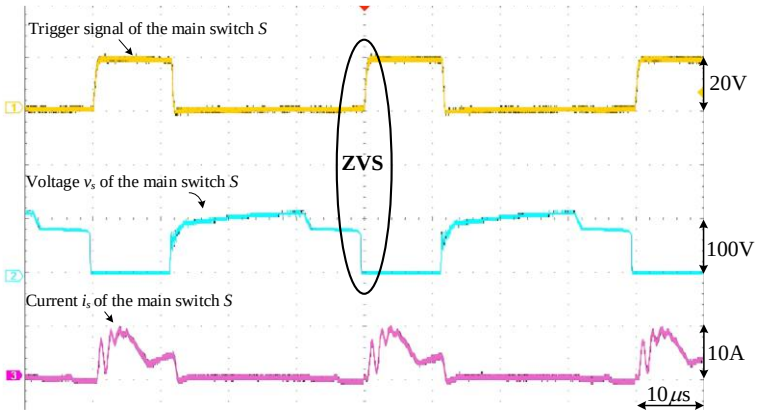

Figure 28. Waveform of the trigger signal, voltage, and current of the main switch *S* under full load (*P*=340W).

 doi:10.20944/preprints202505.1715.v1

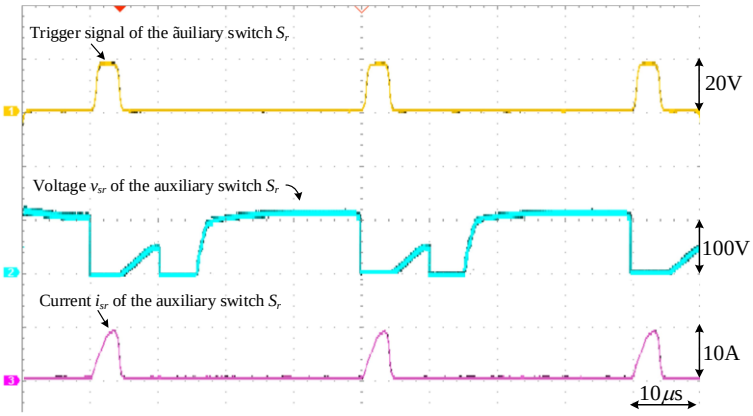

Figure 29. Waveform of the trigger signal, voltage, and current of the auxiliary switch S_r under full load (P=340W).

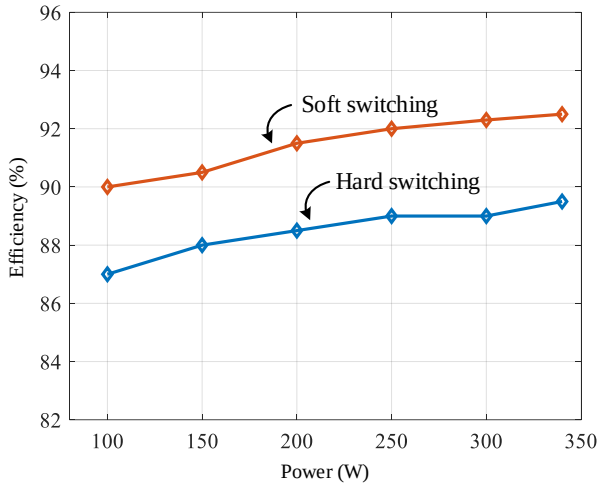

Figure 30. Efficiency comparison between the high step-up soft-switching converter and the hard-switching converter.

6. Conclusion

This paper presents a high step-up soft switching converter topology. Through both simulation analysis and experimental results, it has been demonstrated that the converter achieves zero voltage switching (ZVS) for the main switch. By replacing the traditional energy storage inductor with a coupled inductor and adding a boost circuit, the overall voltage gain of the converter is enhanced, enabling it to achieve a higher voltage output. Additionally, a resonant branch is incorporated to ensure the main switch operates with ZVS, thereby reducing switching losses and switch stress, which in turn improves conversion efficiency. The proposed converter offers advantages such as ease of control via triggering signals, a simple circuit topology, and quantifiable component design parameters. Under different load conditions, the conversion efficiency improves by 3-4%, with a peak efficiency of approximately 93%. Thus, the converter demonstrates excellent conversion performance. This converter is promising for practical applications in photovoltaic module arrays, where it can be used for maximum power point tracking to enhance power generation efficiency.

Author Contributions: K.-H.C. managed the project and completed the soft-switching of the DC-DC converter. K.-H.C. also planned the project and wrote, edited and reviewed the manuscript. T.T.T.B. completed the formal analysis of the high step-up ratio DC-DC converter. T.T.T.B. was also responsible for the software program and validation of the experimental results. All authors have read and agreed to the published version of the manuscript.

Funding: The authors gratefully acknowledge the support and funding of this project by National Science and Technology Council, Taiwan, under the Grant Number NSTC 113-2221-E-167-035.

 doi:10.20944/preprints202505.1715.v1

Institutional Review Board Statement: Not applicable.

Informed Consent Statement: Not applicable.

Data Availability Statement: This study did not report any data.

Conflicts of Interest: The authors of the manuscript declare no conflicts of interest.

Nomenclature

Acronyms

ZVS	zero voltage switching
DC	direct current
AC	alternating current
CCM	continuous conduction mode

Symbols

V_i	the input voltage
V_o	the output voltage
P_i	the input power
P_o	the output power
D	duty cycle between [0;1]
T	the switching period of converter
t_{on}	the switch conduction time within one cycle
t_{off}	the switch off time within one cycle
t_d	delay time
t_α	an additional time delay
t_{DSr}	the operating time of the auxiliary switch
N	turns ratio of coupling inductor
N_1 , N_2	the number of turns in the first and second coils
G	the conversion ratio of the high voltage ratio soft switching converter
f	switching frequency
S	main switch
i_S	the current through the main switch S
v_S	the voltage across the main switch S
S_r	auxiliary switch
i_{Sr}	the current through the auxiliary switch S_r
v_{Sr}	the voltage across the auxiliary switch S_r
L_1 , L_2	the primary side and secondary side of the coupled inductor
i_{L1} , i_{L2}	the current through the primary and secondary sides of the coupled inductor
I_{L1} , I_{L2}	the constant current through the primary and secondary sides of the coupled inductor
v_{L1} , v_{L2}	the voltage across the primary and secondary sides of the coupled inductor
L_r	resonant inductor
i_{Lr}	the current through the resonant inductor L_r
v_{Lr}	the voltage across the resonant inductor L_r
D , D_1 , D_2	fast diodes
i_D , i_{D1} , i_{D2}	the current through the fast diode D , D_1 and D_2
C_o	filter capacitor
C_1	resonant capacitor
i_{C1}	the current through the resonant capacitor C_1
v_{C1}	the voltage across the resonant capacitor C_1
C_2	energy storage capacitor
i_{C2}	the current through the energy storage capacitor C_2
v_{C2}	the voltage across the energy storage capacitor C_2
R	output load

 doi:10.20944/preprints202505.1715.v1

Z_o resonance impedance
ω_o resonance frequency

References

1. Hart, D.W. *Introduction to Power Electronics*, 2nd ed.; Pearson Educ. Taiwan Ltd.: Taipei, Taiwan, 2002; pp. 211–220.
2. Park, D.; Lee, H. Improvements in Light-load Efficiency and Operation Frequency for Low-voltage Current-mode Integrated Boost Converters. *IEEE Trans. Circuits Syst. II Exp. Briefs* **2014**, *61*, 599–603.
3. Park, K.B.; Moon, G.W.; Youn, M.J. Overview of High-step-up Coupled-inductor Boost Converters. *IEEE J. Emerg. Sel. Top. Power Electron.* **2016**, *4*, 689–704.
4. Sathyan, S.; Suryawanshi, H.M.; Ballal, M.S.; Shitole, A.B. Soft-switching DC–DC Converter for Distributed Energy Sources with High Step-up Voltage Capability. *IEEE Trans. Ind. Electron.* **2015**, *62*, 7039–7050.
5. Hassan, W.; Soon, J.L.; Lu, D.D.; Xiao, W. A High Conversion Ratio and High-efficiency Bidirectional DC–DC Converter with Reduced Voltage Stress. *IEEE Trans. Power Electron.* **2020**, *35*, 11827–11842.
6. Zheng, Y.; Brown, B.; Xie, W.; Li, S.; Smedley, K. High Step-up DC–DC Converter with Zero Voltage Switching and Low Input Current Ripple. *IEEE Trans. Power Electron.* **2020**, *35*, 9426–9429.
7. Chao, K.H.; Jheng, Y.C. A Soft-switching Coupled Inductor Bidirectional DC–DC Converter with High Conversion Ratio. *Int. J. Electron.* **2017**, *105*, 164–190.
8. Luo, P.; Liang, T.J.; Chen, K.H.; Chen, S.M. High Step-up DC–DC Converter with Active Switched Inductor and Voltage Doubler Based on Three-winding Coupled Inductor. In Proceedings of the IEEE Applied Power Electronics Conference and Exposition (APEC), Houston, TX, USA, 20–24 March 2022; pp. 731–736.
9. Schmitz, L.; Martins, D.C.; Coelho, R.F. Generalized High Step-up DC–DC Boost-based Converter with Gain Cell. *IEEE Trans. Circuits Syst. I Reg. Pap.* **2017**, *64*, 480–493.
10. Santra, S.B.; Chatterjee, D.; Siwakoti, Y. Coupled Inductor Based Soft Switched High Gain Bidirectional DC–DC Converter with Reduced Input Current Ripple. *IEEE Trans. Ind. Electron.* **2023**, *70*, 1431–1443.
11. Yang, F.; Li, C.; Cao, Y.; Yao, K. Two-phase Interleaved Boost PFC Converter with Coupled Inductor under Single-phase Operation. *IEEE Trans. Power Electron.* **2020**, *35*, 169–184.
12. Sathyan, S.; Suryawanshi, H.M.; Ballal, M.S.; Shitole, A.B. Soft-switching DC–DC Converter for Distributed Energy Sources with High Step-up Voltage Capability. *IEEE Trans. Ind. Electron.* **2015**, *62*, 7039–7050.
13. Powersim. *PSIM User Manual*, Jan. 2023. Available online: https://powersimtech.com/wp-content/uploads/2021/01/PSIM-User-Manual.pdf (accessed on 30 April 2025).
14. Texas Instruments. *TMS320F2809 Datasheet*, Sep. 2022. Available online: https://www.ti.com/lit/ds/symlink/tms320f2809.pdf (accessed on 30 April 2025).
15. Chao, K.H.; Huang, B.Z.; Jian, J.J. An Energy Storage System Composed of Photovoltaic Arrays and Batteries with Uniform Charge/Discharge. *Energies* **2022**, *15*, 2883.
16. Narasimharaju, B.L.; Dubey, S.P.; Singh, S.P. Coupled Inductor Bidirectional DC–DC Converter for Improved Performance. In Proceedings of the International Conference on Industrial Electronics, Control and Robotics, Kakinada, India, 27–29 December 2010; pp. 1–5.